Experimental and Numerical Investigations of Constraint Effect on Deformation Behavior of Tailor-Welded Blanks

Yanhua Li and Jianping Lin

Tailor-welded blanks (TWBs) have been considered as a productive sheet forming method in automotive industries. However, formability of TWBs is reduced due to different properties or thicknesses of the blanks and is a challenge for manufacturing designers. The plastic capacity of TWBs is decreased even when the material and thickness are the same. The constraint effect of the laser weld (including weld and heat-affected zone) material in the forming process of similar TWBs is a key problem to be solved in the research, development and application of thin-sheet TWBs. In this paper, uniaxial tensile tests with full-field strain measurement by digital image correlation and Erichsen tests are performed to investigate the constraint effect on deformation behavior and explore the mechanism of decreasing formability of similar TWBs. In addition, finite element models are conducted under ABAQUS code to further reveal the phenomenal behavior of the constraint effect. The results of the base material and welded blanks are compared for characterizing the differences. Furthermore, in order to better understand this mechanism, theoretical and numerical investigations are employed and compared to interpret the constraint effect of laser weld on the deformation behavior of TWBs. An index is proposed to quantify the constraint effect. Results show that the constraint effect of laser weld appears in both stretch forming and drawing of TWBs. Strain paths are approaching the plane strain condition as compared to the monolithic blank due to the constraint effect. Constraint effect is a major factor affecting the formability of TWBs when the failure occurs away from the weld seam.

Nomenclature	
BM	Base material
CZ	Critical zone
DIC	Digital image correlation
FE	Finite element
FEM	Finite element method
FLD	Forming limit diagram
HAZ	Heat-affected zone
LDH	Limit dome height
SMSG-TWBs	Same material and same gage tailor-welded blanks
TWB	Tailor-welded blank
WZ	Weld zone

1. Introduction

In recent years, tailor-welded blanks (TWBs) have been considered as an effective method for producing lightweighting components in automotive industry. TWBs allow assigning proper material and/or thickness while reducing costs and weight. In Body-In-White manufacturing shop, stamping ability or capacity of sheet metal has always been an important issue. However, due to dissimilar thicknesses/strengths combinations of base material (BM), formability of TWBs is reduced in comparison with that of BMs (Ref 1). Therefore, the deformation behavior and formability of TWBs always attract much attention.

Over the past two decades, a number of studies have focused on the formation of TWBs, particularly the laser-welded blanks. Most studies in literature ascribe the decrease of formability to two major aspects: one is the discrepancy in BMs, and the other is low ductility of weld seam and heat-affected zone (HAZ). Azuma et al. (Ref 1) studied the mechanical properties of TWBs in three standard forming operations, namely stretch forming, stretch-flangeability, and deep drawability. In stretch forming condition, it was found that the weld seam ductility is the limiting factor when the weld seam is oriented parallel to

the major stretch axis, while the formability of the weaker BM is the limiting factor when the weld is normal to the stretch axis. Shi et al. (Ref 2) performed tensile tests of TWBs, and it was reported that the TWBs show significantly higher strength and lower elongation than the base metal. Chan et al. (Ref 3) investigated SPCC steel sheet TWBs with different thickness ratios of 2 (0.5 mm/1.0 mm), 1.67 (0.6 mm/1.0 mm), and 1.25 (0.8 mm/1.0 mm). The experimental results showed that both the level of the forming limit curve and the minimum major strain value decrease with the increasing thickness ratio. This implies that the higher the thickness ratio, the lower the formability of the TWBs. Cheng et al. (Ref 4) studied the stainless steel (AISI 304) TWBs with different dimensions, thickness combinations, and welding orientations. The results indicated that the thinner part of TWBs dominated the majority of deformation, and the FLD of TWB is similar to the FLD of the parent metal. The effects of different welding orientations on the forming performance of TWBs were not negligible. Sun (Ref 5) proposed a concept of integrated strength ratio (ISR).

Yanhua Li and **Jianping Lin,** School of Mechanical Engineering, Tongji University, Shanghai 201804, China. Contact e-mails: liyanhua3544@126.com and jplin58@tongji.edu.cn.

Theoretical model of ISR couples three factors that affect the deformation behavior of TWBs, including strength coefficient of material, real-time thickness, and strain hardening parameter. The results showed that rational matching of initial blank thickness and material property parameters can decrease the integrated strength ratio and reduce deformation non-uniformity of TWB, and thus can improve the formability of TWB in stamping process.

In most studies mentioned above, external performance of the deformation behavior of TWBs was mainly presented from several aspects, such as material strength combination, thickness ratio, hardening properties, and ductility. Nevertheless, a question may arise that whether the formability of TWBs with same material and same gage (SMSG-TWBs) reduces compared to that of monolithic blank? What is the mechanism of the decrease in formability of TWBs? The underlying reasons for these questions remain unknown. To answer them, some researchers began to explore fundamental causes of the forming characteristics of TWBs. Investigations on TWBs from a viewpoint of inhomogeneous structure and heterogeneous material were performed recently.

Lockwood et al. (Ref 6, 7) studied local and global mechanical responses of friction stir-welded AA-2024 using experimental and finite element (FE) techniques. Tensile testing and digital image correlation (DIC) were used to obtain the full-field strain distributions in the transversely loaded weld joint, as well as the local constitutive behavior of the various weld regions. The results indicated that local properties tend to cause a non-uniaxial stress state in the weld region. They established that the amount of constraint developed within the weld, during tensile loading, was primarily limited by specimen thickness. Combination of full-field local strain measurement and numerical modeling is a promising technique for the study of weld. Leitão et al. (Ref 8) also recognized the effect of local properties on the mechanical behavior of weld joints. It was concluded that the constitutive behavior (stress-strain curves) of different weld regions can be assessed from local strain fields using DIC. The effect of inhomogeneous constitutive properties of weld materials was recently explored by Song et al. (Ref 9, 10). They believed that the inhomogeneous properties of weld materials contribute to larger effects on the formability of TWBs made from identical BM than that made from dissimilar ones. Considering the inhomogeneous hardening data of weld materials in simulation, more accurate results could be predicted especially for TWBs made from identical base sheets.

In order to evaluate the effect of two parameters, namely geometric discontinuity and presence of weld region, on the formability of TWBs, Abbasi et al. (Ref 11) performed limiting dome height tests and FE simulations. The studied TWB was a blank with thickness ratio (TR) of 1.5. Real and machined blank without weld region TWB specimens were prepared through laser welding and machining. It was found that the decisive factor in decreasing the dome height of TWBs is geometric discontinuity and the effect of weld zone is about 6%. However, this conclusion is in contradiction to the behavior of SMSG-TWBs (Ref 1), which considers that the presence of weld zone is a vital factor for the deformation of TWBs. Azuma (Ref 1) pointed out that the forming height of longitudinal and transverse SMSG-TWBs (with a strength ratio of 1.0) decreases about 30 and 8%, respectively, compared to that of the parent material. Moreover, the maximum forming height of TWBs with thickness ratio of 1.5 is approximately 60% of that of the thicker parent material. With the develop-ment of research on TWB, there is a growing awareness that the constraint effect of weld was accounted for inhomogeneous structure and local mechanical properties of TWBs. Thus far, there have been a few studies on this topic. Zhan et al. (Ref 12, 13) investigated the constraining effects of the weld and HAZ material on the tube bend formability by simulating FE model in ABAQUS®.

Constraint effect of weld on the forming of TWBs was also found by Sorgente et al. (Ref 14) when they investigated the mechanical and technological behavior of AZ31 magnesium alloy laser-welded joints. The results show that a restriction of formability of butt welded joints was observed; the strain path generated by the presence of the weld was steeper than that of the BM and it is closer to the plane strain condition. Similar results (in terms of change in the slope of the strain path) were also found by Leitão et al. (Ref 8) in tensile tests carried out on aluminum friction stir welds. They correlated the change in the slope of strain path to the existence of constraints in the deformed area and/or to severe anisotropic conditions inside it.

Hu et al. (Ref 15) investigated the effect of the microstructure heterogeneity on the tensile plastic deformation characteristics of friction stir-welded (FSW) 2024 aluminum alloy. They indicated that the deformation of the weld would be constrained by the adjacent BM. In addition, tangential stresses arise at contact surfaces as a result of constraining plastic strains by the weld metal.

Mohebbi et al. (Ref 16) had already realized the constraint effect of weld when developing a new model to predict the Forming Limit Diagrams (FLDs) of TWBs. The model was derived by modification of the Marciniak and Kuczynski (MK) analysis and imposing the weld constraints to deformation state of each blank at each strain increment. It was demonstrated that this model provides a close prediction of FLD of TWBs, when necking occurs far from the weld line at a region out of HAZ and close to it so that it is affected by the weld line constraints.

Global and local deformation behavior of similar laser-welded joints were investigated and analyzed through tensile specimens of SMSG-TWBs and BM with the aid of DIC strain measurement by Li et al. (Ref 17). Except for the specimen of 0° TWB, yield strengths of the specimens of TWB and BM are almost identical. The global hardening behavior of 45° and 30° TWB is lower than that of others. As for local properties, constraint effect is formed due to the existence of laser weld. Also, previous research (Ref 18) investigated mechanical properties of laser weld seam of SMSG-TWBs by combining the rule of mixture and DIC as well as miniature size uniaxial tensile test. Then, based on these mechanical properties, formability of TWBs and monolithic blank was evaluated by performing Erichsen cupping tests numerically and experimentally. Nevertheless, this paper focuses on mechanical properties of weld seam and forming simulations rather than on the constraint effect (Ref 18).

In spite of these successful investigations discussed above, there are limited studies directed to investigate the constraint effect of SMSG-TWBs. It is highly desirable to conduct more work for a better understanding of this phenomenon since it also widely exists in other similar welding joints, such as electron beam welded joints and other butt welded joints. The purpose of this study is to reveal the mechanism of reduced formability of SMSG-TWBs, using experimental and numerical approaches. TWBs are fabricated from DC05 steel sheet with same material and thickness. The tensile deformation characteristics of the longitudinal and transverse weld direction TWB

specimens are examined using Vic-3D (Correlated Solutions®) full-field strain measuring system. Biaxial tension deformation of TWBs is conducted by Ericshen test. Both the tensile and biaxial tension deformation are simulated using the FE code software ABAQUS. Moreover, this paper tends to interpret the constraint effect theoretically and experimentally. Evaluation of its effect on the formability of TWBs and the proposed methods for improving the formability of TWBs are discussed.

2. Materials and Methods

2.1 Materials

The present investigation is focused on DC05 low-carbon steel sheet with blank thickness of 1.0 mm. Chemical composition of material is shown in Table 1. Laser welding was carried out using a CO_2 laser source with a power of 4 kW at a welding speed of 7 m/min. Standoff distance was set as 0.5 mm. Shielding gas was Ar and flow rate was 20 L/min. All TWBs were fabricated with welding direction parallel to the rolling direction. Specimens without any weld imperfections were selected as testing samples. Miniature tensile specimens of BM and weld seam were tested

Table 1 Chemical composition of thin steel sheet used in the present study

Material	C	Mn	P	S	Alt	Ti
DC05	≤ 0.008	≤ 0.30	≤ 0.020	≤ 0.020	≤ 0.015	≤ 0.20

Table 2 Mechanical property parameters of DC05 BM and laser weld seam

Material	Yield strength, MPa	Tensile strength, MPa	K, MPa	n
DC05 BM	137.7	378.3	522.62	0.2395
Weld seam	318.0	387.4	441.37	0.0599

K and n represent strength coefficient and strain hardening exponent, respectively
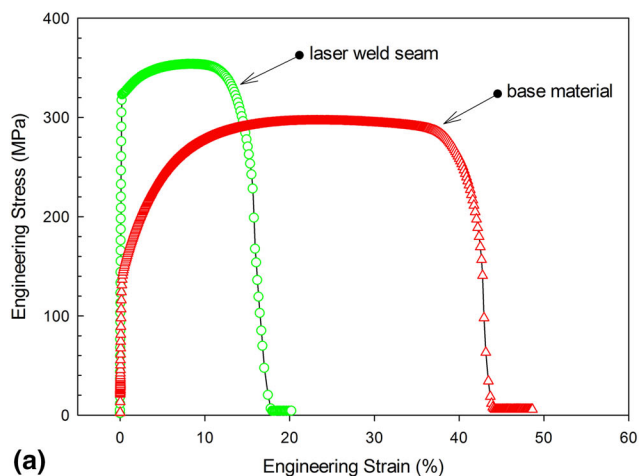
after laser welding. Engineering and true stress-strain curves were obtained, as shown in Fig. 1 and Table 2.

Figure 1(a) and 1(b) show the engineering and true stress-strain curves of BM and weld seam, respectively. Tensile tests of BM and weld seam were obtained at a static strain rate of $0.001 \ s^{-1}$ using miniature tensile specimens. It is noted that the yield stress of weld seam is higher than that of BM, while the strain hardening parameter and elongation were lower than that of BM, as indicated in Table 2.

2.2 Tensile Behavior Testing of TWBs Based on DIC

Deformation behavior of the TWBs was investigated by standard tensile tests. Dimensions of the tensile test specimens of TWBs are shown in Fig. 2. Width and gage length of specimen are 12.5 and 75 mm, respectively. Total length of
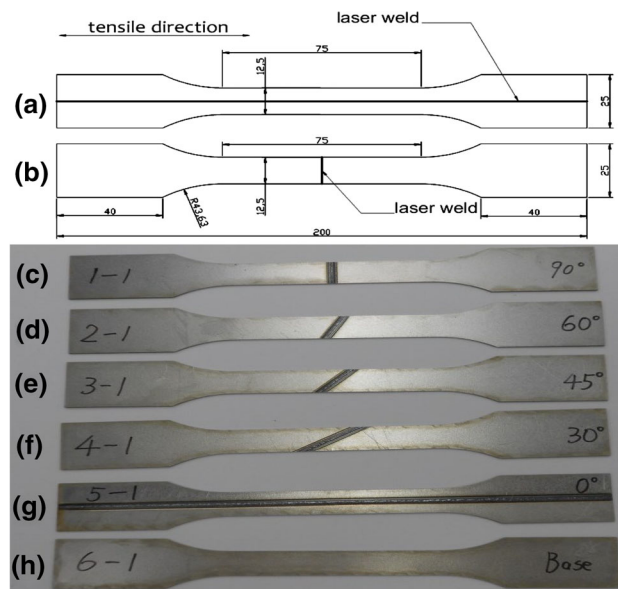

Fig. 2 Schematic of the tensile test specimens of TWBs: (a) dimensions of longitudinal weld direction specimen, (b) dimensions of transverse weld direction specimen, (c) transverse weld direction specimen (90°), (d) 60° direction specimen, (e) 45° direction specimen, (f) 30° direction specimen, (g) longitudinal weld direction specimen (0°), and (h) BM specimen (unit in mm)
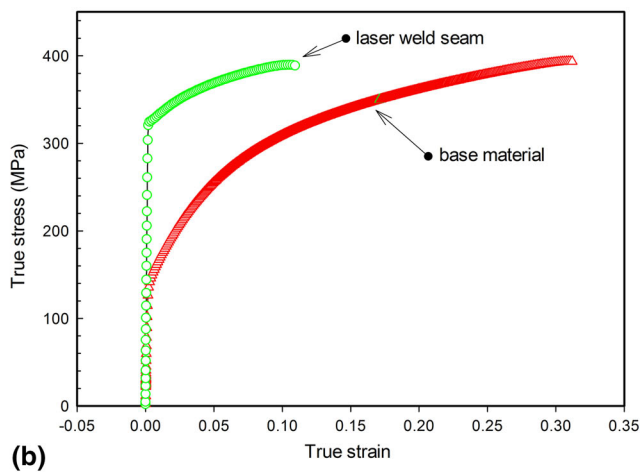

Fig. 1 Stress-strain curves of BM and weld seam: (a) engineering stress-strain curves and (b) true stress-strain curves

specimen is 200 mm. Figure 2(a) gives a schematic of a full-size longitudinal tensile specimen, with the weld centered in the gage section and the loading axis parallel to the welding direction. Figure 2(b) represents a schematic of transverse tensile specimen with welding direction normal to the tensile direction. Figures 2(c) to 2(h) show the real TWB tensile testing specimens with 90°, 60°, 45°, 30°, and 0° weld orientations. To measure sheet metal strain in the tensile test, a strain and force measurement system was built. Figure 3 shows the experimental setup. A universal testing machine (ZWICK-050) was used for measuring the conventional engineering strain-stress curve. In order to measure full-field true strain, a

DIC system (Vic-3D, Correlated Solutions®) with two high-speed cameras was placed in front of the sample on a stable tripod. Tensile test specimens used in the experiment were fabricated according to the ASTM-E8/E8M (Ref 19) standards. Random speckle patterns were sprayed on the object surface, first with white spray paint and then with black spray paint.

2.3 Biaxial Stretch Testing of TWBs and BM

Erichsen cupping test was employed here to evaluate the ability of plastic deformation in stretch forming. This test consists of forming an indentation by pressing punch with

Fig. 5 FE model for the tensile test of transverse weld direction specimen

Fig. 6 3-D FE model for the Erichsen cupping test of TWBs

Fig. 3 Correlated Solutions® 3-D DIC system integrated on a ZWICK 050 universal tensile testing machine. Top left: schematic of tensile test machine. Bottom right: schematic of the DIC measurement system
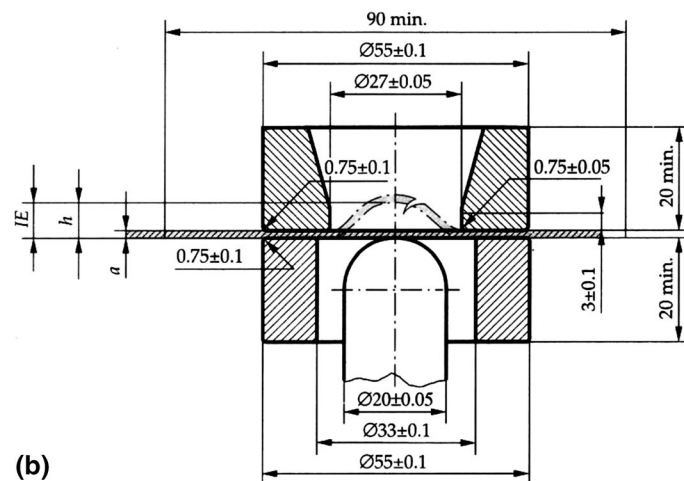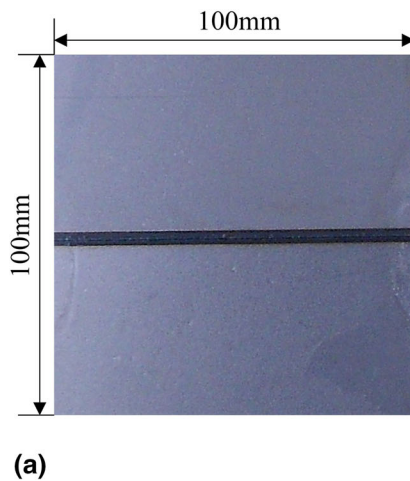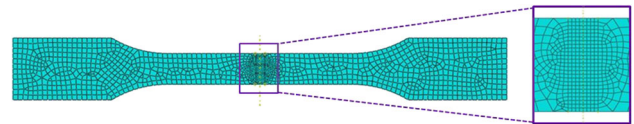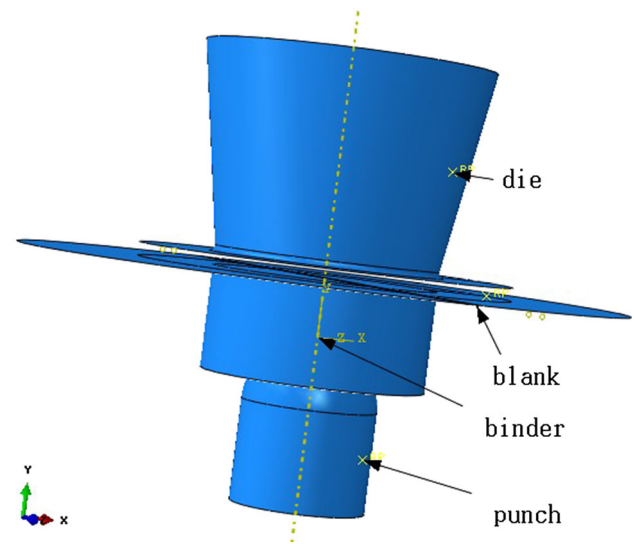

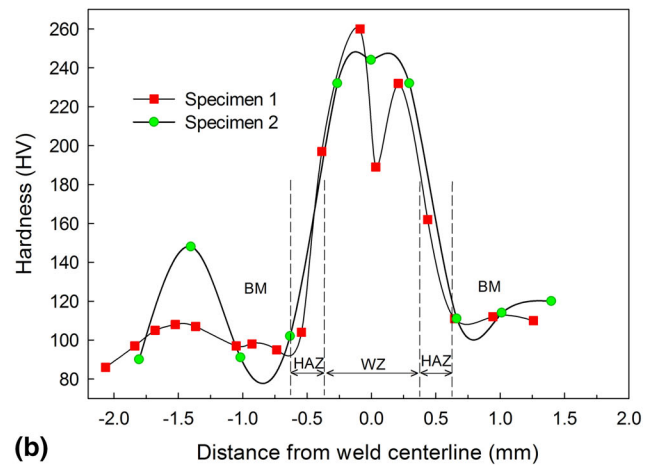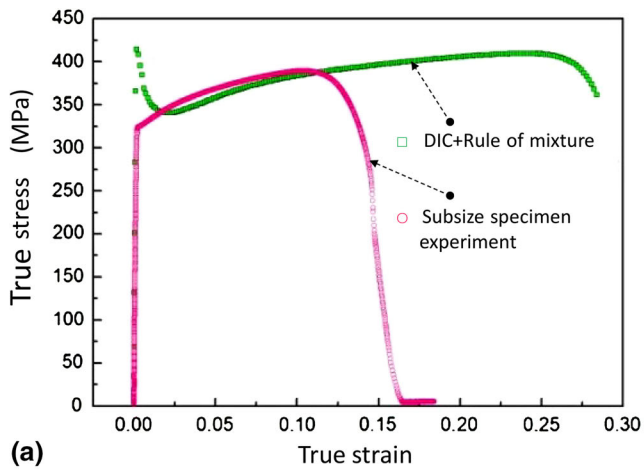**Fig. 4** The Erichsen cupping test: (a) specimen and (b) apparatus (unit in mm)

Fig. 7 Mechanical properties of BM and laser weld: (a) true stress-strain curves obtained by sub-size specimen and DIC and (b) Vickers hardness distributions of two TWBs
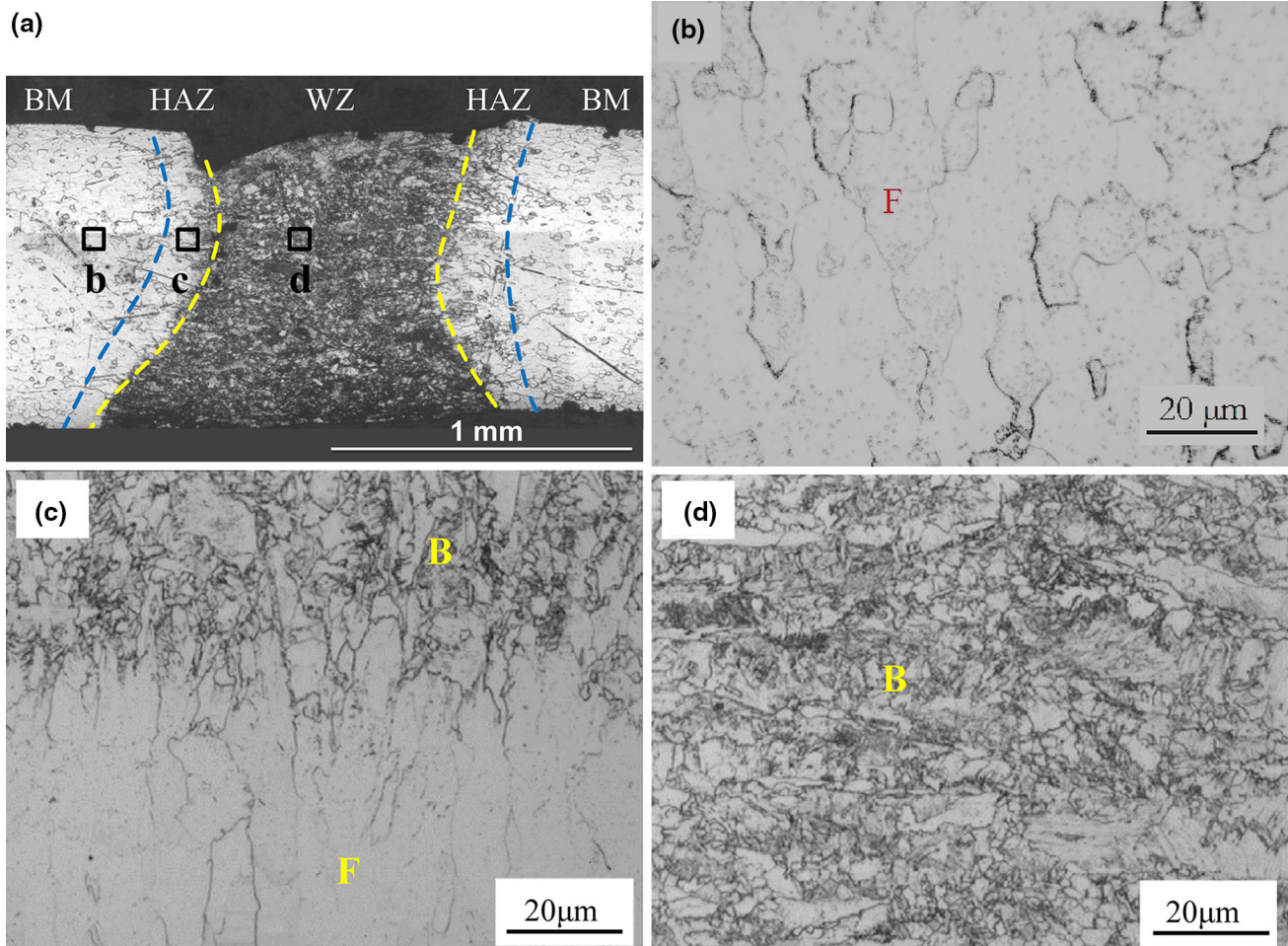

Fig. 8 Optical micrographs showing microstructure change of the DC05 welded joint: (a) overall view of the cross section, (b) BM, (c) HAZ, and (d) WZ (where F: ferrite, B: binite)

spherical end against a test piece clamped between blank holder and die, until a through crack appears. Depth of the cup was then measured. Test set-up for cupping test is shown in Fig. 4 according to the international standards ISO 20482. The welded specimen was carefully placed to locate the weld line at the center of the dome punch. A 20-mm-diameter hemispherical punch was used with a velocity of 10 mm/min. To minimize friction between blank and punch, lubricating grease was

Table 3 Comparison of constraint effect parameters of all samples

Samples	Constraint scale (mm)	Constraint degree
90°TWB	18	0.06
60°TWB	16	0.05
45°TWB	30	0.07
30°TWB	34	0.10
0°TWB	...	Fracture strain 0.42
BM	...	Fracture strain 0.59

utilized in the contact face. Clamping holder force was 10 KN during the whole testing to assure a pure stretching condition.

2.4 Microhardness, Microstructure, and Fractography Experiments

Vickers microhardness was determined using a load of 500 g and a dwell time of 12 s. All the microhardness values presented in this study were an average of three series of values taken on the same specimen. Microstructure and fracture examinations were done using an optical microscope and a JEOL S-3400N scanning electron microscope (SEM), respectively.

2.5 Finite Element Modeling and Simulations

The advantage of numerical analysis is determination of deformation history of TWB which cannot be fully obtained through experiment, such as strain path and stress distribution. In order to study the constraint effect of laser weld, numerical approaches are needed for comparing with the experimental results. Here, FE analyses were done by a commercially available code ABAQUS 6.9. Mechanical properties and stress-strain curves of BM and weld seam used in FEM are shown in Table 2 and Fig. 1. In the present work, four-node shell element S4R was used for blank because of lower computational time. For tensile test model of TWBs, element size of weld zone was refined to 0.5 mm, which is shown in Fig. 5. The element size was 2 mm in other zone. As for the model of the Erichsen cupping test, forming tools were modeled as analytical rigid body, including punch, die, and binder (see Fig. 6). Friction coefficient was assumed to be 0.1 between forming tools and blank. The influence of residual stresses due to welding was not considered in the numerical models.

3. Results and Discussion

3.1 Mechanical Characterization of BM and Weld Seam

In the process of laser welding, weld zone (WZ) and HAZ are formed. The microstructures of WZ and HAZ are different from that of BM due to the high power input of laser welding equipment. As a result, heterogeneous mechanical properties are developed within tailor-welded joint. Hence, it is crucial to identify the local mechanical properties of different zones for determining the deformation behavior and analyzing the constraint effect of TWBs. These local properties include yield stress, tensile stress, elongation, as well as hardness. For simplicity, due to their small gage, WZ and HAZ were treated as a whole, which is called as "weld seam" in this paper.

In addition to the tensile curves obtained from subsize specimens, stress-strain curve of weld seam was also calculated by standard specimen using DIC and rule of mixture. Stress-strain curves of miniature and DIC method specimens are depicted in Fig. 7(a). The maximum strain of weld seam in miniature specimen at necking is nearly 0.12. However, the limit strain of weld seam is almost 0.25 in the standard specimen, as shown in Fig. 7(a). The miniature specimen of weld seam is also called "weld only" specimen. With 4 mm in width and lower hardening parameter, the "weld only" specimen necked and fractured quickly. One possible reason is that, in the standard specimen, BM is presented in both sides of weld seam. The necking of weld seam was limited by the adjacent BM in the tensile test of the specimen (i.e., Fig. 2a and 2g). With increased tension force and decreased cross-sectional area, the stress value of weld seam was raised. Consequently, the mechanical properties of weld seam in subsized and standard specimens were dissimilar, although both subjected same deformation mode.

A higher hardness in the weld zone is observed in the Vickers micro-hardness test of the TWB cross section, as compared to that of BM in Fig. 7(b). It is found that hardness value of the weld seam was approximately 2.0 times higher than that of the BM. The average hardness values of weld seam and BM are 240 HV and 120 HV, respectively. The width of laser weld seam is approximately 1.25 mm, including HAZ and WZ.

Based on the studies above, the basic characteristics of TWB are higher yield stress and higher hardness as well as lower hardening parameter of weld seam compared to that of BM. These discrepancies could be associated with variable microstructures of WZ and HAZ. The effect of mechanical parameters on the constraint effect will be interpreted in later sections.

3.2 Microstructure and Fractography

The overall view of weld cross section of the welded joint is shown in Fig. 8(a). It can be seen that the weld cross section exhibits a heterogeneous structure across various regions of the welded joint, including WZ, HAZ, and BM. More detailed microstructure changes are shown in Fig. 8(b) to 8(d). According to microstructure images and hardness results, the approximate boundaries of the three regions were marked in Fig. 8(a) using dashed lines.

The microstructure of the BM (see Fig. 8b) is characterized by ferrite matrix, which is in accordance with the properties of this low-carbon steel. Figure 8(c) shows the microstructure of HAZ, including both ferrite and bainite, where the volume fraction of bainite is about 25%. In the weld zone, almost fully bainite microstructure (see Fig. 8d) is observed. Compared to the BM, a higher volume fraction of hard phases is found in the WZ and HAZ, which results in an increase in hardness. The microhardness of the WZ is even higher (average microhardness 240 HV) than that of the BM (average microhardness 120 HV), as is shown in Fig. 7(b).

According to the descriptions above and the processes of laser welding, the local microstructures and properties at any point within the welded joint are generally determined by the thermal cycle experienced at that location. Hardening in WZ and HAZ results in changes of local strength and ductility, which significantly affects the overall tensile properties, deformation behavior, and failure mechanisms of the welded joints (see Fig. 8a to 8c).
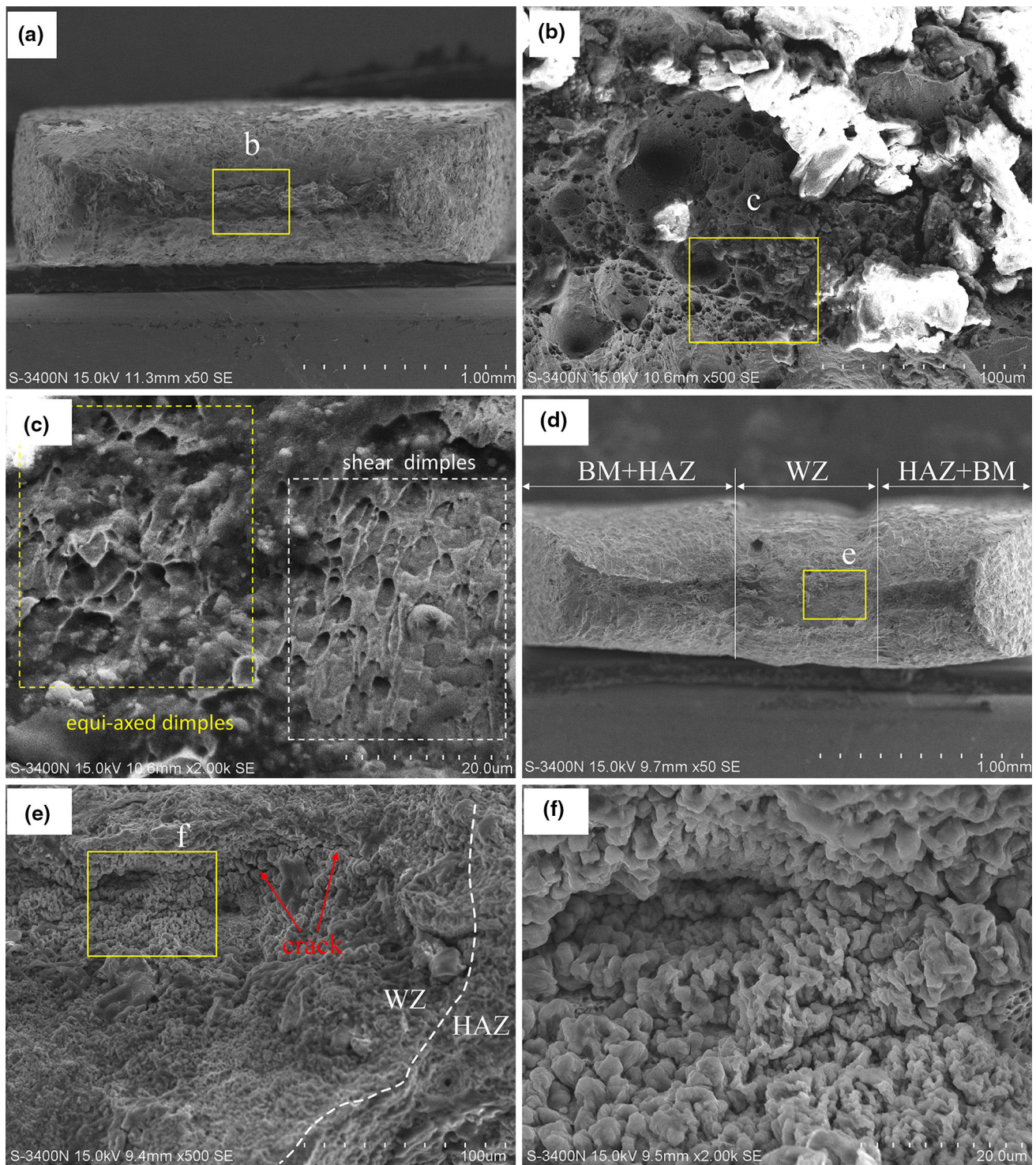
Fig. 9 Fractographs of the BM and welded joint: (a) overall view of the fracture section of BM, (b) fracture surface at a higher magnification in the propagation area as indicated by a rectangular box in (a), (c) fracture surface at a higher magnification in the propagation area as indicated by a rectangular box in (b), (d) overall view of the fracture section of WZ and HAZ, (e) fracture surface at a higher magnification in the propagation area as indicated by a rectangular box in (d), (f) fracture surface at a higher magnification in the propagation area as indicated by a rectangular box in (e)

Fracture surfaces of the BM and welded joint were investigated through tensile specimens subjected to quasi-static tension. The cross section of welded joint consisted of WZ, BM, and HAZ. Figure 9 shows some typical SEM images of fracture surfaces of BM and welded joint after tensile tests at a strain rate of 1×10^{-3} s^{-1}. Ductile type of failure mode is observed by a combination of both equiaxed and shear dimples for BM fracture surface (see Fig. 9(a) to 9(c)). In Fig. 9(c), cup-like dimple rupture is the main feature of fracture surface of BM, representing ductile type of fracture mode. The left part of
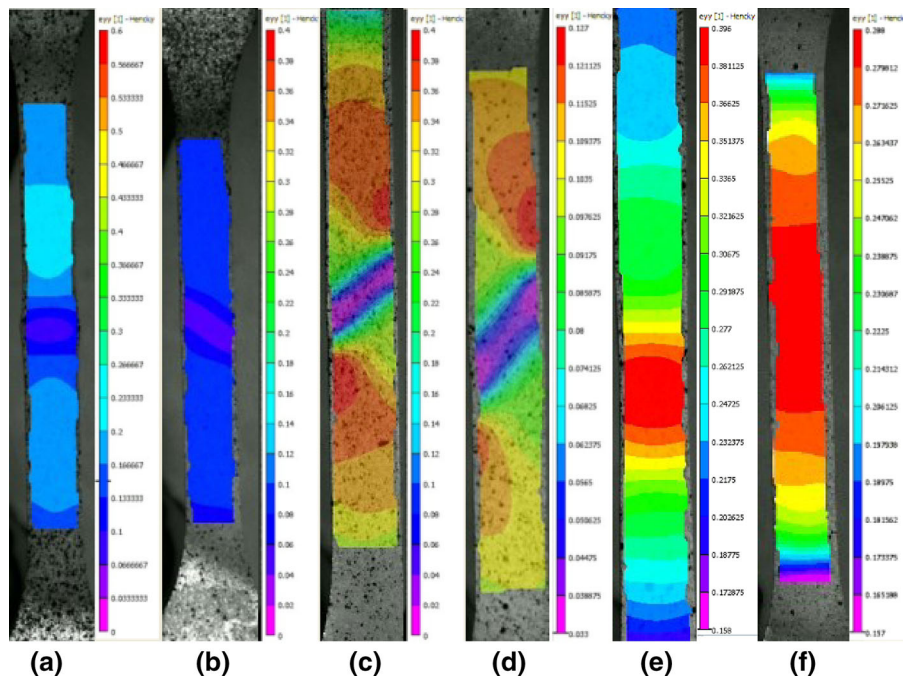
Fig. 10 Strain maps of tensile test specimens of TWBs and BM: (a) 90°, (b) 60°, (c) 45°, (d) 30°, (e) 0°, and (f) BM

Fig. 9(c) shows dimpled impressions of equiaxed appearance. Dimples having elongated parabolic shape, namely shear dimples, are observed in the right part of Fig. 9(c). This indicates the occurrence of shearing motion in conjunction with the simple tensile load.

The SEM images in Fig. 9(d) to 9(f) show the fracture surfaces of welded joint. Near the HAZ, a local zone at the WZ marked "e" is selected from Fig. 9(d). In Fig. 9(e), WZ and HAZ are separated by a dashed line. It can be concluded from Fig. 9(e) that almost no dimples are observed in the WZ. The fracture surface of WZ is characterized by brittle failure mode. Fracture surface at a higher magnification in the propagation area is shown in Fig. 9(f). Cracks appear in this zone. The fractographic observations corresponded well to the relatively low ductility of WZ (Fig. 7). However, in the HAZ, dimples are found again. Based on the observations above, it could be summarized that a part of the microstructures is transformed, and mechanical properties are changed during the processes of laser welding and cooling. Consequently, the weld seam of TWB is characterized by higher yield stress, higher hardness, and lower hardening parameter compared to that of BM for the steel studied in this article.

3.3 Tensile Behavior Testing of TWB

Tensile behavior testing was performed using both DIC-based experiments and simulations. Figures 10(a) to 10(f) show strain maps of tensile test specimens of 90°, 60°, 45°, 30°, and 0° TWBs and BM, respectively. In Fig. 10(a) to 10(d), the laser welds are less deformed than the material nearby. Plastic deformation is concentrated in the BM zone of TWBs. Failure presents in the BM. However, with regard to the 0° TWB and BM specimens, iso-stress condition is satisfied and the strain distributions are similar in both cases. Besides, the strain in the weld is the same as the material nearby shown in Fig. 10(e). For the tensile test specimen of BM, the distribution of major

strain is uniform, as shown in Fig. 10(f). This phenomenon is common in tensile testing of monolithic metal sheets. Simulated maximum and minimum strain rates are approximately 0.26 and 0.18 s^{-1}, respectively, in the six tensile simulation models.

DIC method can be used to calculate the evolution of deformation fields at selected intervals, from the beginning of the testing to the fracture of the specimen. Therefore, it is possible to extract strain states of a surface, a line or a point. In order to investigate the global and local strain distributions of different zones, major strains ε_{yy} are plotted at different stages. The weld direction with respect to tensile direction (Y direction) is defined in Fig. 11(a). Transverse and longitudinal weld specimens represent that weld direction is normal and parallel to tensile direction Y. The selected line is located at the center of specimen (see Fig. 11a), namely center symmetry line.

Figures 11(b) to 11(g) represent the strain distributions of TWBs and BM. In each figure, abscissa represents distance along tensile direction, and vertical represents major strain. Strain distributions were plotted every 100 frames (200 ms/frame) until crack occurred. For the TWB samples from 90° to 30°, a "U-valley" is observed at the middle position which means smaller strain.

Compared with BM tensile specimen, the strain distribution is less uniform in 90° weld tensile specimen (Fig. 11b). In the length range of 20 mm, between 10 mm distance right from the origin and 10 mm distance left from the origin, the strain is smaller than the zones far away from the length range and a U-shaped curve is observed. At the position of the origin where the center of weld nugget is located, the strain reached its minimum value. It is also found from the Fig. 11(b) that, for the TWBs, the average strain in laser weld region is almost half of that in other regions.

Although the strain distribution was rather uniform compared to that of BM specimen, the maximum strain in 0° tensile specimen is lower than that of BM specimen, as can be seen in
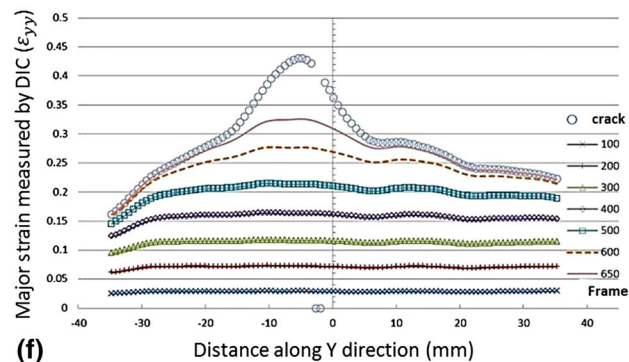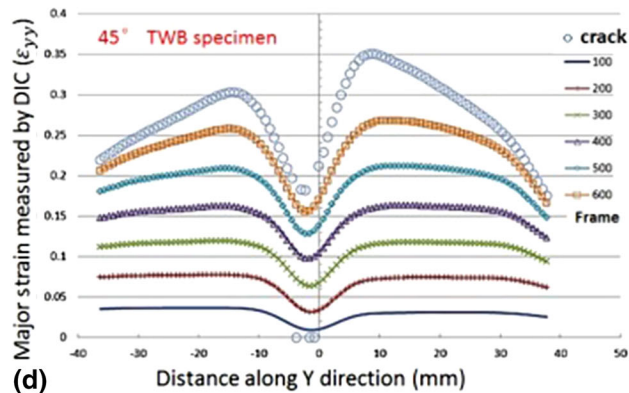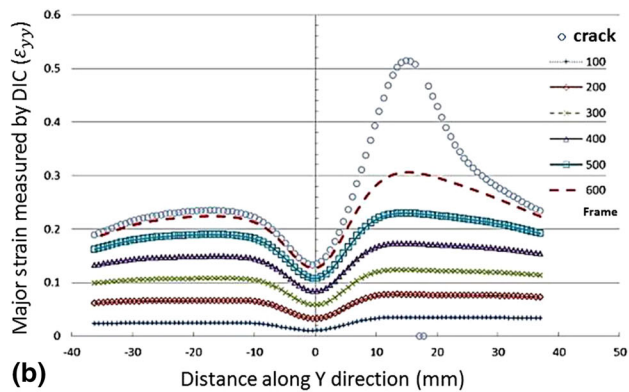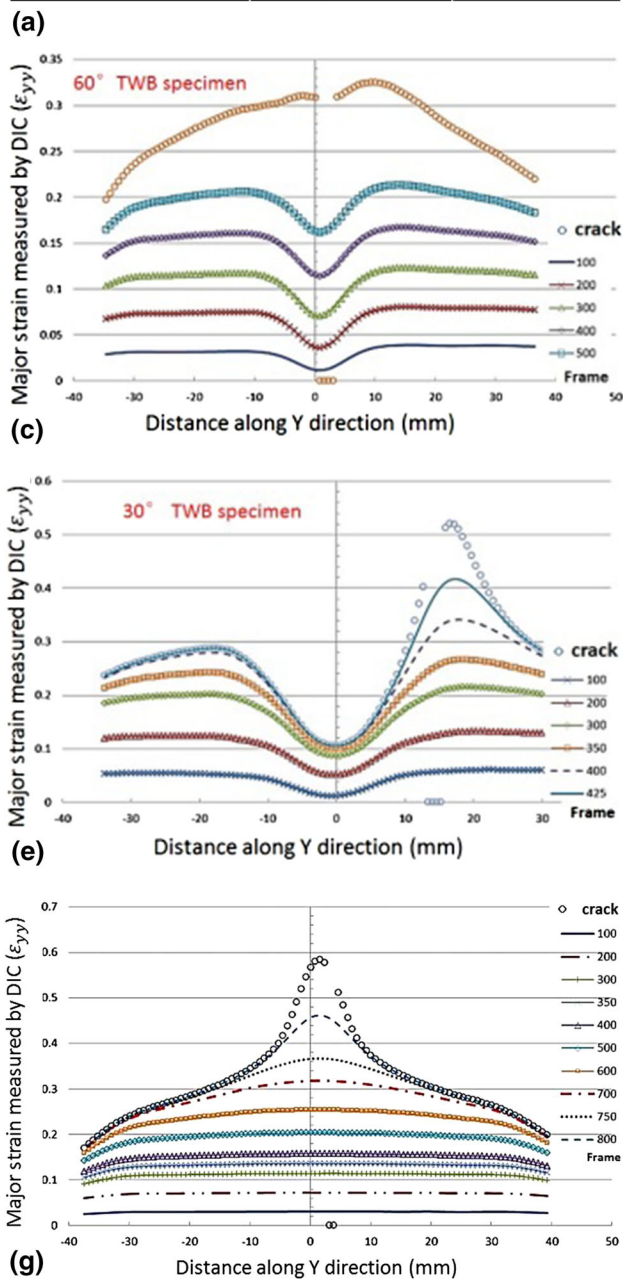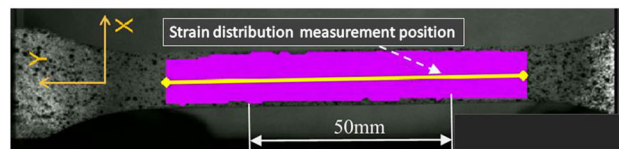
Fig. 11 Strain distributions along the length direction of the specimens

Fig. 11(f) and 11(g). This phenomenon can be interpreted by the lower elongation of the laser weld.

Scale and degree in the "U-valley" are used for characterizing the constraint. Firstly, in Fig. 11, for the TWB tensile specimens with weld seam varying from 90° to 30° toward the direction of tensile, a 'U-valley' was observed at the middle position. Constrain scale is defined here by the distance between the two top points of the "U-valley". And constrain degree is defined by the strain difference between the top point and lowest point of the "U-valley". Secondly, for the TWB

tensile specimen with weld seam parallel to the direction of tension and BM specimen, constraint degree is defined by fracture limit strain of laser weld seam and BM, respectively. But constrain scale is not applicable for these specimens. Table 3 gives the comparison of the two parameters of all samples. It can be found that the constraint scale and constraint degree values of 30° TWB specimen are largest among four TWB specimens. Constraint effect is developed within the TWB due to the laser weld seam. The deformation of the zone near the weld is constrained by the harder laser weld seam. This
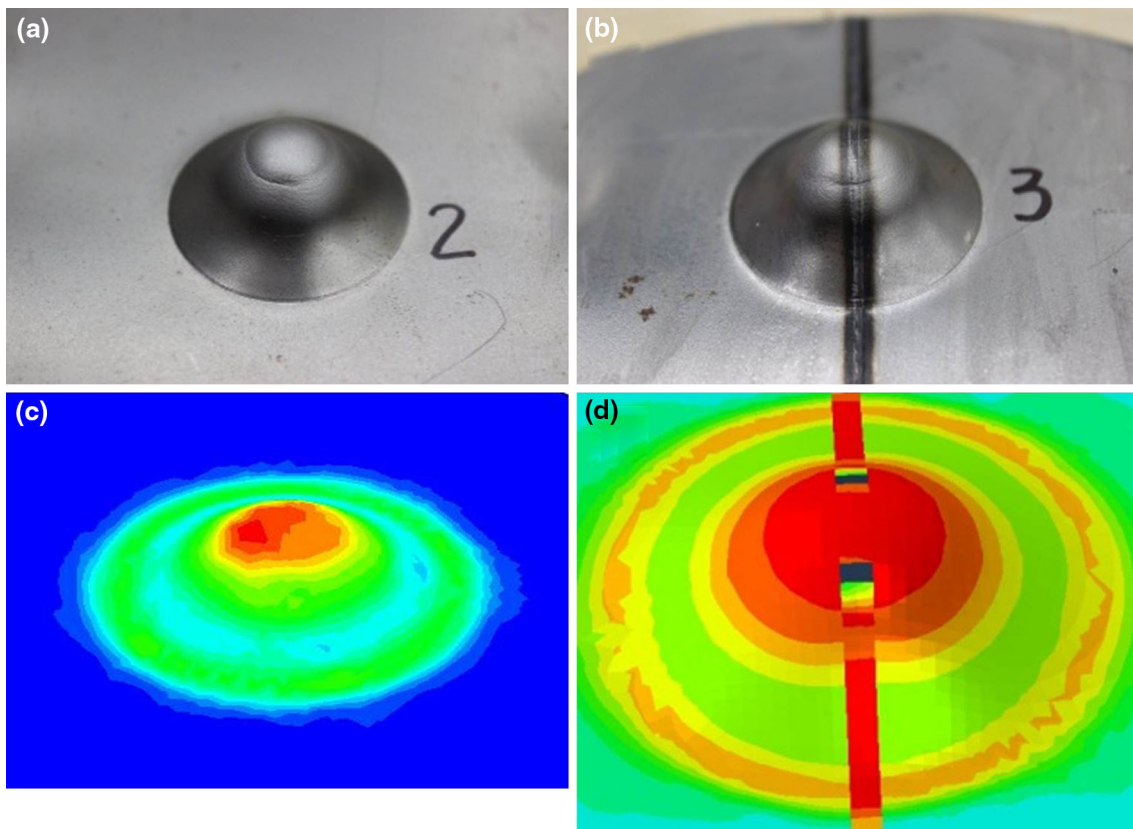
Fig. 12 Experimental and numerical results of Erichsen tests of TWBs: (a) BM, (b) TWBs, (c) FE-simulation of BM, and (d) FE-simulation of TWBs

constraint effect is owing to the strength mismatch between laser weld seam and BM. Characterizations for constraint, which come from the observations and analyses of experimental and numerical results, are proposed according to the deformation mode of TWBs in sections 3.3 and 3.4.

3.4 Biaxial Stretch Testing

Erichsen test and simulation results are exhibited in Fig. 12. As shown in Fig. 12(a) and 12(b), failure occurs in the laser weld seam of TWBs. Failure heights for the specimen of BM and TWB are 13.6 and 12.5 mm, respectively. It can be observed that simulation results are in good agreement with the test results. In order to obtain the mechanism of constraint effect, BM specimen with homogeneous thickness was also tested for comparing, as is shown in Fig. 12(a) and 12(c). The selected section for investigating is along the symmetric axis of the dome and is normal to the weld, as is presented in Fig. 13. In consideration of the major strain direction, the symmetry line perpendicular to the weld line was selected for investigating the constraint. Along this section, the directions of major strain of BM are the same. Coordinate origin was located in the weld seam. Strain ratio (the ratio of minor strain to major strain) and strain path, as well as strain evolution, were studied for further explaining how the constraint effect works and to what extent it can have affect. Due to the limitation of experimental test for strain ratio and strain history, numerical simulation was utilized for getting the data step by step.

Figure 14 provides the major and minor strain distributions of the defined section of cupping test specimens for BM and
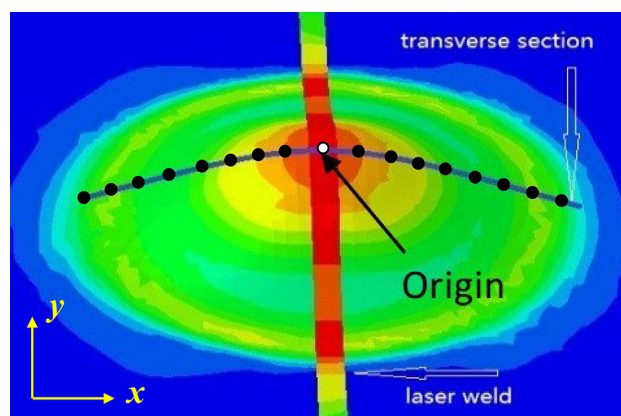

Fig. 13 Schematic representation of the selected section

TWB before fracture. Within the length scale of approximately 13 mm, between 7 and 20 mm distance left from the origin, both distributions are similar. However, from the point which is 7 mm distance left to the origin to the origin point, the strain distributions are quite different. Although both major strain distributions have a similar tendency, the maximum major strain value of TWB specimen is larger than that of BM. In addition, opposite trend of minor strain distributions is observed.

Strain ratio distributions of BM and TWB are described in Fig. 15. At the origin, the strain ratio is 1 for BM specimen, which means equivalent biaxial tension state. Nevertheless, the
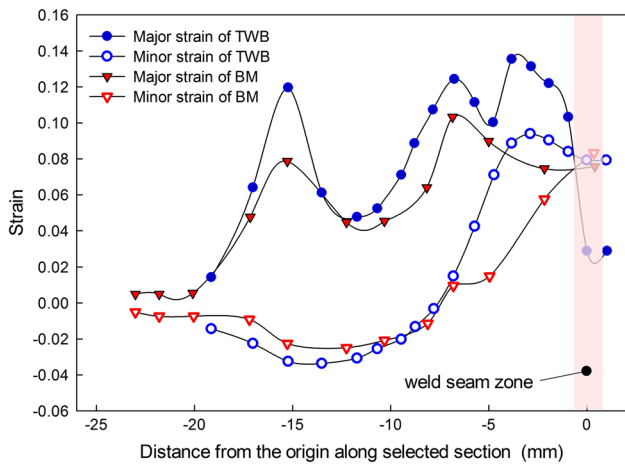
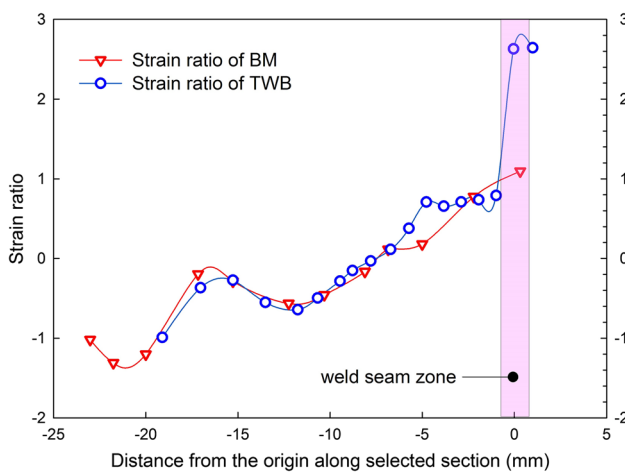**Fig. 14** Major and minor strain distributions of the selected transverse section of cupping tests on BM and TWB

Fig. 15 Strain ratio distributions of the selected transverse section of cupping tests on BM and TWB
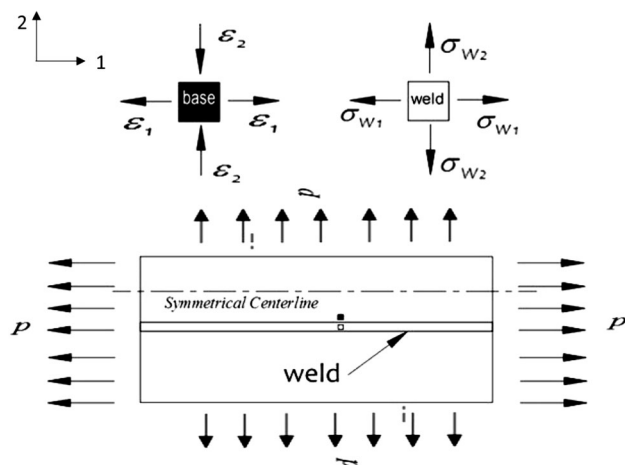

Fig. 16 Schematic representation of deformation analysis on TWB

strain ratio is about 2.6 (ratio of strain along weld and strain normal to weld) for TWB specimen at the origin. In addition, the strain ratio of adjacent region (within the 5 mm length
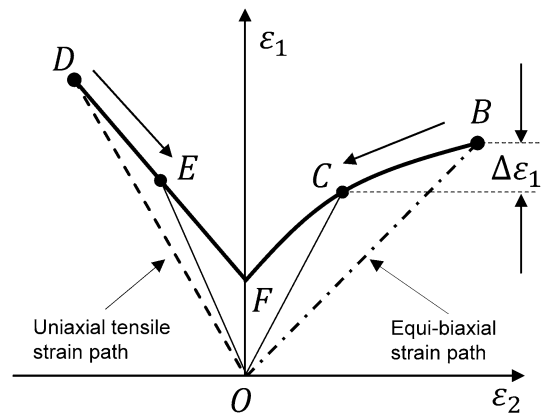

Fig. 17 Schematic of Strain path shift to plane strain condition within CZ

range) of weld seam is approximately 0.7. For the BM specimen, within the same region stated above, the strain ratio distribution is monotonic smoothly. Therefore, it could be concluded that strain ratio in the BM zone near weld seam is changed due to the constraint effect.

3.5 Effect of Constraint Effect on Formability of TWB

Reduced formability of TWB is always an important issue focused by automotive industries. The formability of TWB can be affected by tailoring in two aspects: firstly, the weld seam fails before BM due to low ductility and formability of laser weld seam; secondly, change of strain path (strain ratio) and its history due to constraint applied by laser weld seam (including weld zone and HAZ).

When necking or failure is out of the weld seam, the constraint effect plays an important role in the strain path or strain ratio. During deformation, the BM blanks which are different from laser weld seam in material properties are constrained toward the direction of weld seam. Therefore, the strain ratio and deformation history of TWB specimen would be different from that of BM specimen, especially in the region near weld seam in TWB. Figure 16 presents the deformation characteristics analyses of TWB and BM. Firstly, considering that the TWB is deformed under biaxial stretch deformation condition. Due to the compatibility constraint in the direction 1, strain is the same in both weld seam and BM blank (Eq 1). However, in the zone (defined as CZ) near weld seam, strain of BM in direction 2 ($\varepsilon_2^{\text{base}}$) is larger than that of BM in direction 1 ($\varepsilon_1^{\text{base}}$). Therefore, the strain ratio in CZ would be smaller than that of the BM ($\beta^{\text{TWB}} < \beta^{\text{base}}$).

$$\varepsilon_1^{\text{weld}} = \varepsilon_1^{\text{base}}. \tag{Eq 1}$$

And then, it is considered that the TWB is subjected to uniaxial tensile in direction 2. As a result of constraining by weld seam with higher material strength, $\varepsilon_1^{\text{base}}$ in CZ is smaller than that of monolithic BM blank. In consideration of the negative strain ratio value in this deformation mode, therefore, the strain ratio of CZ would be larger than that of the BM ($\beta^{\text{base}} < \beta^{\text{TWB}}$).

An index is proposed here to describe the degree of constraint effect imposed by weld seam on the BM.

$$\varphi = \frac{\beta^{\text{base}}}{\beta^{\text{TWB}}}. \qquad\qquad (\text{Eq } 2)$$

Equation (2) represents a ratio between two strain ratios: the strain ratio (β^{base}) in CZ of BM blank and the strain ratio in that of TWB (β^{TWB}). It means that strain in zone adjacent to weld seam is different from the strain in the same zone of monolithic blank under same forming condition. In other words, the strain ratio and deformation history of TWB may be different from that of BM. For example, it displays no constraint effect when φ equals 1. The parameter φ only associates with three main factors. First one is the yield strength discrepancy between BM and weld seam. The second factor is the position of the zone relative to weld seam. Far from the weld seam, effect of constraint gradually diminishes and forming behavior approaching to monolithic blank. Relative geometry of weld seam is the last factor that affects φ.

It is well known that bad ductile weld zone would reduce the overall formability of TWB. Here, only failures away from weld zone are considered and analyzed. The constraint effects of weld seam on formability of TWB are demonstrated in Fig. 17. Curve DEF and curve FCB are the forming limit curves of BM monolithic blank. Dash-dot line OB and dashed line OD represent equi-biaxial and uniaxial tensile strain paths of CZ in the deformation of BM, respectively. In case of TWB, the forming limit curves of BM in TWB are still curve DEF and curve FCB. Nevertheless, the strain paths of CZ in TWB shift to the plane strain condition with smaller limit strains, from line OB to line OC in the first quadrant and from line OD to line OE in the second quadrant. Consequently, this phenomenon of strain path shifts caused by constraint effect of weld seam can properly interpret the decreasing formability of similar TWBs (see ε_1 in Fig. 17). In a word, constraint effect is a major factor for the decrease in formability of similar TWB when failure is out of weld seam.

4. Conclusions

In this paper, mechanical properties of BM and weld seam were investigated experimentally by tensile tests and Erichsen stretching tests. Microstructure and fractography were assessed for characterizing the heterogeneous structure of TWB. Constraint effect of the laser weld seam on deformation of similar TWB was obtained and analyzed by FE simulations and experiments. Effect of constraint effect on the formability of TWB was discussed. The following are the main conclusions from the results obtained in this investigation.

(1) The weld seam of TWB is characterized by higher yield stress, higher hardness, and lower hardening parameter compared to that of BM for the steel studied in this article. Ductile and brittle fracture modes were observed in the BM and weld zone, respectively.

(2) For the TWB tensile specimens with weld seam varying from 90° to 30° toward the direction of tensile, plastic deformation is concentrated in BM zone of TWBs. For the TWB tensile specimen with weld seam parallel to the direction of tension, deformation is constrained by limit strain of laser weld seam. Under stretching forming mode, strain ratio and deformation history of the BM zone near weld seam in TWB specimen are different to that of the same zone for BM specimen. The constraint is characterized by the sizes of the U-valley and strain ratio in the tensile and stretching forming modes, respectively.

(3) Strain path in the BM zone near weld seam for TWB is approaching the plane strain condition compared with that of the same zone for monolithic blank as a result of constraint effect. An index is proposed to describe the degree of constraint. According to the theoretical analyses of both tensile and stretching of TWB, constraint effect is a major factor affecting the formability of TWBs when failure is out of weld seam.

References

1. K. Azuma, K. Ikemoto, K. Arima, H. Sugiura, and T. Takasago, Sheet Metals in Forming Processes. *Proc. 16th Biennial Congr.*, ASM International, Metals Park, OH, 1988, p 205–215
2. M. Shi, K. Pickett, and K. Bhatt. Formability Issues in the Application of Tailor Welded Blank Sheets. *SAE Technical Paper 930278*, 1993. doi:10.4271/930278
3. S.M. Chan, L.C. Chan, and T.C. Lee, Tailor-Welded Blanks of Different Thickness Ratios Effects on Forming Limit Diagrams, *J. Mater. Process. Technol.*, 2003, **132**(1–3), p 95–101
4. C.H. Cheng, L.C. Chan, and C.L. Chow, Weldment Properties Evaluation and Formability Study of Tailor-Welded Blanks of Different Thickness Combinations and Welding Orientations, *J. Mater Sci.*, 2007, **42**(15), p 5982–5990
5. D. Sun, "*Research on the Formability of Tailor-Welded Blank Based on Integrated Strength Ratio*". Ph.D. Dissertation. Tongji University, 2009
6. W.D. Lockwood, B. Tomaz, and A.P. Reynolds, Mechanical Response of Friction Stir Welded AA2024: Experiment and Modeling, *Mater. Sci. Eng. A*, 2002, **323**, p 348–353
7. W.D. Lockwood and A.P. Reynolds, Simulation of the Global Response of a Friction Stir Weld Using Local Constitutive Behavior, *Mater. Sci. Eng. A*, 2003, **339**, p 35–42
8. C. Leitão, I. Galvão, R.M. Leal, and D.M. Rodrigues, Determination of Local Constitutive Properties of Aluminium Friction Stir Welds Using Digital Image Correlation, *Mater. Des.*, 2012, **33**, p 69–74
9. Y. Song, L. Hua, D. Chu, and J. Lan, Characterization of the Inhomogeneous Constitutive Properties of Laser Welding Beams by the Micro-Vickers Hardness Test and the Rule of Mixture, *Mater. Des.*, 2012, **37**, p 19–27
10. Y. Song and L. Hua, Influence of Inhomogeneous Constitutive Properties of Weld Materials on Formability of Tailor Welded Blanks, *Mater. Sci. Eng. A*, 2012, **552**, p 222–229
11. M. Abbasi, M. Ketabchi, A. Ramazani, Mohammad Abbasi, and U. Prahl, Investigation into the Effects of Weld Zone and Geometric Discontinuity on the Formability Reduction of Tailor Welded Blanks, *Comput. Mater. Sci.*, 2012, **59**, p 158–164
12. M. Zhan, D. Hongfei, J. Liu, N. Ren, H. Yang, H. Jiang, K. Diao, and X. Chen, A Method for Establishing the Plastic Constitutive Relationship of the Weld Bead and Heat-Affected Zone of Welded Tubes Based on the Rule of Mixtures and a Microhardness Test, *Mater. Sci. Eng. A*, 2010, **12**, p 2864–2874

13. N. Ren, M. Zhan, H. Yang, Z.Y. Zhang, Y.T. Qin, H.M. Jiang, K.S. Diao, and X.P. Chen, Constraining Effects of Weld and Heat-Affected Zone on Deformation Behaviors of Welded Tubes in Numerical Control Bending Process, *J. Mater. Process. Technol.*, 2012, **5**, p 1106–1115

14. D. Sorgente, G. Palumbo, L.D. Scintilla, and L. Tricarico, Evaluation of the Strain Behaviour of Butt Joints on AZ31 Magnesium Alloy Thin Sheets Welded by Nd:YAG laser, *Int. J. Adv. Manuf. Technol.*, 2013, **67**(9–12), p 2753–2763

15. Z.L. Hu, X.S. Wang, and S.J. Yuan, Quantitative Investigation of the Tensile Plastic Deformation Characteristic and Microstructure for Friction Stir Welded 2024 Aluminum Alloy, *Mater. Charact.*, 2012, **73**, p 114–123

16. M.S. Mohebbi and A. Akbarzadeh, Prediction of Formability of Tailor Welded Blanks by Modification of MK Model, *Int. J. Mech. Sci.*, 2012, **61**, p 44–51

17. Y. Li and J. Lin, Evaluation of Global and Local Deformation Behaviors of Similar Laser Welded Joints Using Digital Image Correlation. *SAE Technical Paper 2014-01-0832*, 2014. doi: 10.4271/2014-01-0832

18. Y. Li, J. Lin, and R. Guo, Numerical and Experimental Analysis on the Formability of Tailor Welded Blanks Based on Digital Image Correlation. *AIP Conference Proceedings*, vol. 1567, 2013, p 772–775. doi:10.1063/1.4850084

19. ASTM E8/E8M. Standard test methods for tension testing of metallic materials. ASTM International; 2012